ELSEVIER

First-principles study of adsorption and diffusion on Ge/Si(0 0 1)-(2 × 8) and Ge/Si(1 0 5)-(1 × 2) surfaces

Li Huang [a,*], Guang-Hong Lu [b], Feng Liu [c], X.G. Gong [a]

[a] *Surface Physics Laboratory, Department of Physics, Fudan University, Shanghai 200433, PR China*
[b] *Department of Physics, Beijing University of Aeronautics and Astronautics, Beijing 100083, PR China*
[c] *Department of Materials Science and Engineering, University of Utah, Salt Lake City, UT 84112, USA*

Abstract

Using first-principles total-energy calculations, we have investigated the adsorption and diffusion of Si and Ge adatoms on Ge/Si(0 0 1)-(2 × 8) and Ge/Si(1 0 5)-(1 × 2) surfaces. The dimer vacancy lines on Ge/Si(0 0 1)-(2 × 8) and the alternate S_A and rebonded S_B steps on Ge/Si(1 0 5)-(1 × 2) are found to strongly influence the adatom kinetics. On Ge/Si(0 0 1)-(2 × 8) surface, the fast diffusion path is found to be along the dimer vacancy line (DVL), reversing the diffusion anisotropy on Si(0 0 1). Also, there exists a repulsion between the adatom and the DVL, which is expected to increase the adatom density and hence island nucleation rate in between the DVLs. On Ge/Si(1 0 5)-(1 × 2) surface, the overall diffusion barrier of Si(Ge) along $(\bar{5}0 1)$ direction is relative fast with a barrier of ∼0.83(0.61) eV, despite of the large surface undulation. This indicates that the adatoms can rapidly diffuse up and down the (1 0 5)-faceted Ge hut island. The diffusion is also almost isotropic along [0 1 0] and $[\bar{5}0 1]$ directions.
© 2007 Elsevier B.V. All rights reserved.

Keywords: Density functional calculations; Surface diffusion; Silicon; Germanium

1. Introduction

In recent years, there has been wide interest in understanding and controlling the epitaxial growth of Ge and SiGe alloy films and islands on Si(0 0 1) because of its technological and scientific importance [1,2]. Some key general thermodynamic aspects associated with these systems have been made clear. Due to the 4.2% lattice mismatch between Ge and Si, the growth of Ge film on Si substrate typically proceeds via the Stranski–Krastanov mode. The deposited Ge atoms initially form a wetting layer up to three monolayers (ML), consisting of dimer vacancy lines (DVLs) perpendicular to the dimer rows because of the compressive strain in the overlayer. The surface thus gradually changes

its reconstruction from the Si(0 0 1) (2 × 1) structure to a Ge/Si(0 0 1)-(2 × N) pattern [3,4], with N saturated at ∼8 for a 3 ML Ge coverage. Three-dimensional (3D) coherent islands then grow on top of the 3 ML Ge wetting layer to further relieve the accumulated misfit strain. In particular, scanning tunneling microscopy (STM) studies have identified that the transition from 2D to 3D growth is characterized by the formation of hut islands preferentially bounded by {1 0 5} facets [5,6].

Epitaxial growth usually proceeds under conditions far away from thermodynamic equilibrium. Thus, a detailed knowledge of the growth kinetics is highly desirable to further improve our understanding. In particular, underlying atomistic processes that occur on surfaces, such as adsorption, diffusion, and nucleation, play an essential role in the evolution of the surface structures and morphologies [7]. To date, however, little theoretical work has been devoted to the adatom kinetics on Ge/Si(0 0 1)-2 × N [8,9] and on Ge/Si(1 0 5) surfaces [10]. Actually, the correct atomic

---

* Corresponding author. Present address: School of Physics, Georgia Institute of Technology, 837 State Street, GA 30332, USA. Tel.: +1 404 894 0892.
E-mail address: lhuang32@mail.gatech.edu (L. Huang).

structure of Ge/Si(105) surface (i.e. the facet on Ge hut island) has not been determined until very recently [11–15]. The very limited knowledge of adatom kinetics (such as surface diffusion) has hindered the further progress in understanding the growth of Ge and SiGe films and islands on Si(001).

In a recent study [16], we have investigated the surface mobility difference between Si and Ge and its effect on growth of SiGe alloy films and islands. The aim of this paper is to present a more detailed adatom kinetics involved in the initial stages of (Si)Ge epitaxial growth on Si(001). We perform a comprehensive first-principles study of the adsorption and diffusion of both Si and Ge adatoms on Ge/Si(001)-(2 × 8) and Ge/Si(105)-(1 × 2) surfaces. We explore the role played by the rebonded missing dimers on Ge/Si(001)-(2 × 8) surface and the alternate S_A and rebonded S_B steps on Ge/Si(105)-(1 × 2) surface in influencing adatom kinetics by comparison with the adatom dynamics on flat or stepped Si(001) surface. On a Ge/Si(001)-(2 × 8) surface, the single fastest diffusion path is over the top of the rebonded DVL. The diffusion anisotropy is thus reversed with respect to that on Si(001) and Ge(001). Also, there exists repulsion between adatoms and DVLs. The adatom diffusion on (105) surface is found to be rather fast, with the overall barrier for Si(Ge) adatom along [$\bar{5}$01] direction being ∼0.83(0.61) eV. The diffusion is almost isotropic along [010] and [$\bar{5}$01] directions, differing from that on Si(001) or Ge(001), where the Si(Ge) adatom diffusion is highly anisotropic with the preferable diffusion taking place along the dimer rows.

2. Computational method

All calculations are performed in the framework of the density functional theory within the local-density approximation to the exchange and correlation energy [17]. The electron–ion interaction is described by ultrasoft pseudopotentials [18]. The Kohn–Sham orbitals are expanded in plane waves with an energy cutoff of 11 Ry. The calculated equilibrium lattice constants for bulk Si and Ge are 5.39 Å and 5.63 Å, respectively, in good agreement with the experimental values (5.429 Å for Si and 5.652 Å for Ge). The

Ge/Si(001) surface is simulated by a repeated slab model in which three Ge layers, three Si layers and ∼10 Å vacuum region are included. The bottom of the slab has a bulk-like structure with each Si atom saturated by two H atoms. The atoms in the surface layer form a 2 × 8 reconstruction containing the DVL, as shown in Fig. 1. The Ge/Si(105) surface is modeled by repeated slab geometry of 12 Ge(105) layer thickness with twofold rotational symmetry axis along the [010] direction, seperated by a vacuum region of ∼11 Å. Although the whole slab is composed of Ge atoms, the lattice constant parallel to the (105) surface is set to that of Si to mimic the role of strain of the Ge(105) layers formed on Si. The two Ge(105) surfaces reconstruct following the rebonded-step (RS) model [12,13], as shown in Fig. 2a. The geometry optimization has been performed for all atoms except for the bottommost H and Si atoms of Ge/Si(001) and the innermost layers of Ge atoms of Ge/Si(105), by conjugate gradient minimization, up to a precision of 10^{-4} eV in total-energy difference and with the forces on the unconstrained atoms being less than 0.01 eV/Å. Brillouin-zones for the Ge/Si(001) and Ge/Si(105) slabs are sampled at a grid of 4 × 1 × 1 and 2 × 2 × 1 Monkhorst–Pack k-point mesh [19], respectively. Tests have been done to make sure that all the results are converged with respect to energy cutoff, system size, and k-point sampling.

On Ge/Si(001) surface, the exact locations and energies of the binding sites are determined by fully relaxing all the atoms (including the adatom) unconstrained, starting from the possible minimum sites with reference to the binding sites on a $p(2 × 2)$ reconstructed Si(001) surface [20,21]. Since there is no experimental and computational evidence for the binding sites of the adatoms on Ge/Si(105) surface, the potential-energy surface (PES) seen by a single Ge(Si) adatom over this surface have been mapped out by minimizing the total energy with respect to the z coordinate of the adatom along with the coordinates of all other atoms over a set of equidistant grid points. The PES of a Ge adatom on Ge/Si(105)-(1 × 2) shown in Fig. 2b is a cubic spline fit to the original data. The local minima are then accurately located by putting the adatom on the interpolated minima and relaxing all atomic positions without
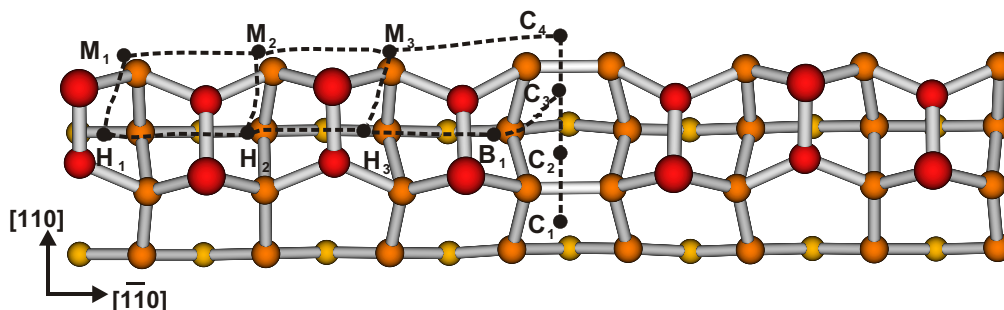
Fig. 1. Top view of the unit cell of Ge/Si(001) surface (i.e. a 3-ML Ge on Si(001)) with (2 × 8) reconstruction. Atoms at lower three layers in the slab model are not shown. Higher atoms are drawn by larger spheres while lower atoms by smaller spheres. The second-layer atoms exposed at DVL are rebonded. The letters and dashed lines indicate the positions of main binding sites and the low-barrier diffusion pathways, respectively.
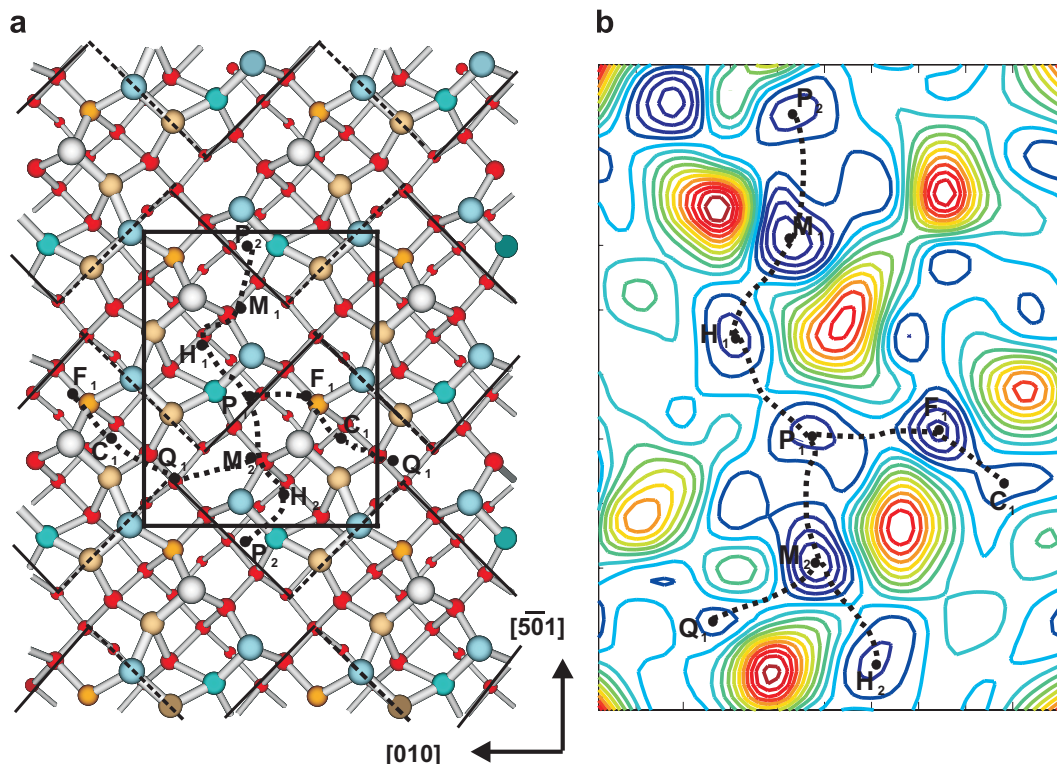
Fig. 2. (a) Top view of the optimized Ge/Si(105) surface (i.e. Ge(105) with the lateral lattice constant of Si) with reconstruction following the rebonded-step model. Higher atoms are drawn by larger spheres while lower atoms by smaller spheres. S_A steps are shown by solid lines, and rebonded S_B steps by dashed lines. The (105) unit cell is outlined by a rectangle with the dimension of $2a \times \sqrt{6.5}a$ (here a is the lattice constant of Si (5.39 Å)). (b) Contour plot of the calculated potential-energy surface of a Ge adatom on Ge/Si(105)-(1×2) surface. The letters and dashed lines indicate the positions of main binding sites and the low-barrier diffusion pathways, respectively.

constraints. The PES for a Si adatom exhibit qualitatively similar features to that of Ge adatoms, at least with respect to the critical points on it. The saddle points between any two minima and hence the diffusion barriers are identified using the nudged elastic band (NEB) method [22].

3. Results and discussion

3.1. Adatom kinetics on Ge/Si(001)-(2×8) surface

The binding sites and diffusion pathways of Si(Ge) adatoms on clean Si(001) surfaces have been unambiguously determined in earlier studies. With the calculated PES for Si(Ge) adatom on Si(001) [20,21] in mind, we perform extensive search of the possible binding sites for Si(Ge) adatom on the (2×8) reconstructed Ge/Si(001) surface in the presence of DVL. The resultant main minimum sites are indicated in Fig. 1. When the adatom is located away

from the DV's, the binding sites on this surface are similar to that on clean Si(001) surfaces. Both Si and Ge adatoms prefer to bind at the subscripted M-type and then H-type sites. The minimum sites directly over the rebonded second-layer dimers exposed at the DV sites (subscripted C's in Fig. 1) form a *shallow* energy channel in the energy surface. The relative adsorption energies of these local minimum sites, with respect to the absolute minima, are given in Table 1.

For each type of adatom (Si or Ge), we focus on the diffusion parallel to the dimer rows, along which the fast diffusion of Si(Ge) adatom on clean Si(001) surface occurs, as well as the diffusion over the top of the DVL (dashed lines in Fig. 1). Figs. 3 and 4 show the potential energies along the different pathways for Ge and Si adatom diffusion on Ge/Si(001) surface, respectively.

The energetics of adsorption in Table 2 and of surface diffusion in Figs. 3 and 4 highlight several interesting

Table 1
Adsorption energies (eV) for Si and Ge adatoms at (local) minimum sites on Ge/Si(001)-(2×8) surface, relative to the global minimum site M_1 for Ge and M_3 for Si

	M_1	M_2	M_3	H_1	H_2	H_3	B_1	$C_{1(2)}$	C_3	C_4
Ge	0.00	0.04	0.09	0.10	0.10	0.15	0.28	0.44	0.37	0.74
Si	0.30	0.36	0.00	0.38	0.37	0.41	0.58	0.70	0.71	1.09
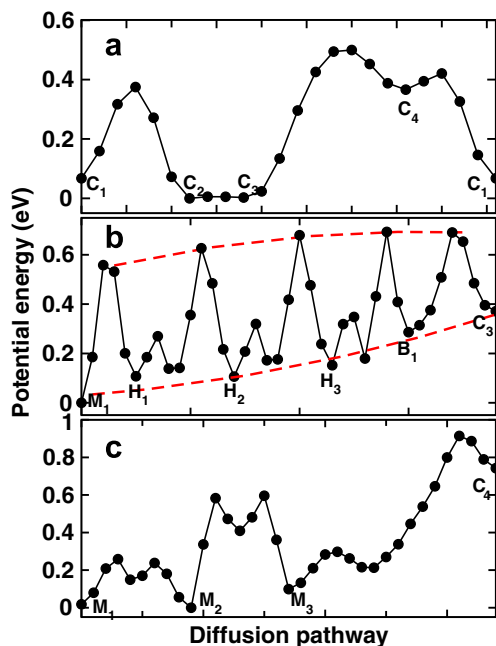
Fig. 3. The potential energies along the different pathways of a Ge adatom on Ge/Si(0 0 1)-(2 × 8) surface, as depicted in Fig. 1. (a) Diffusion pathway over the dimer vacancy lines; (b) and (c) are for the diffusion pathways parallel to the dimer rows with (b) along the top of the dimer row and (c) along the edge of the trough between the dimer rows. The dashed lines in (b) are quadratic fit to the potential energies of the minima and saddle points.
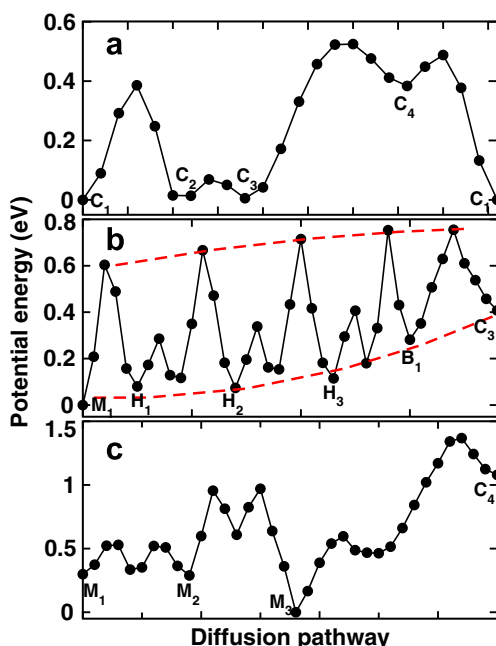
Fig. 4. Same as Fig. 3 for the potential energies along the different pathways of a Si adatom on Ge/Si(0 0 1)-(2 × 8) surface.

Table 2
Adsorption energies (eV) for Si and Ge adatoms at (local) minimum sites on Ge/Si(1 0 5)-(1 × 2) surfaces, relative to the global minimum M site

	M	F	H	P	Q	C
Ge	0	0.069	0.298	0.288	0.406	0.408
Si	0	0.145	0.309	0.322	0.507	0.420

the rebonded DVL, following the pathway $C_1C_2C_3C_4$ with the activation barrier of 0.49 eV for Ge and 0.52 eV for Si adatoms (Figs. 3a and 4a). The diffusion anisotropy is therefore reversed with respect to that on clean Si(0 0 1) and Ge(0 0 1) surface. However, this diffusion path with the lowest overall activation barrier is not necessarily the dominant mass transport way, given the facts that there is only a small number (1/8) of such paths (vacancy lines) in the surface, and the binding is much weaker on top of the DVL than on the flat terrace. Second, the energy barrier for diffusion along the top of the dimer rows is 0.56(0.60) eV for Ge(Si) adatom with $M_1 \rightarrow H_1$ as the rate-limiting step (Figs. 3b and 4b), close to those on unstrained Ge(0 0 1) surface [21]. This is because, although the Ge film is "nominally" strained by ~4.2%, the (2 × 8) reconstruction has largely relaxed the strain in the surface, making it like an unstrained surface. Calculations have shown that the (2 × N) reconstruction actually overcompensates the compressive strain leading to a tensile surface stress in Ge(0 0 1)-(2 × N) [4,23]. Third, as the adatom on top of the dimer row approaches the dimer vacancy, its potential energy (and hence effectively its chemical potential) continues to rise while the barrier at each individual step decreases slightly (see dashed lines in Figs. 3b and 4b), indicating that there is an effective repulsive interaction between adatom and vacancy. This feature agrees well with our previous calculation of strain dependence of Ge adatom diffusion on Ge(0 0 1) [21], which revealed that the adatom binding and activation energies decrease with the uniaxial tensile strain along the dimer rows. Fourth, for diffusion along the trough edge between the dimer rows (Figs. 3c and 4c), the activation barriers are quite sensitive to the local tilting of the dimers, with a lower barrier being encountered when passing the down dimer atom [24,25]. An additional relatively large energy barrier appears near the rebonded missing dimers. This feature was also predicted by Yu and Oshiyama for Ge adatom diffusion on Ge/Si(0 0 1) (2 × 4) surface [9].

The above results have some interesting implications on the initial nucleation and epitaxial growth of (Si)Ge films on Si(0 0 1) surface. As the Ge overlayers (the wetting layers) grow, the strain-driven alignment of DV's results in 2 × N reconstruction. The subsequently deposited Ge(Si) adatoms will mostly land on the flat terraces in between the DVLs. Consequently, the effective repulsive interaction between adatoms and vacancies and the additional energy barrier induced by the DVLs may increase the adatom concentration in between the DVLs and hence enhance the island nucleation probability to roughen the surface. This

features. First, the diffusion behavior of both adatoms on the surface is significantly affected by the presence of the DVL. The single fastest diffusion path is along the top of

may lead to formation of pre-nucleus [23,26] for subsequent formation of hut islands.

3.2. Adatom kinetics on Ge/Si(105)-(1×2) surface

To facilitate the discussion we first illustrate the detailed structure of the rebonded Ge/Si(105) surface, as shown in Fig. 2a. The surface is partitioned by zigzag steps into nanoscale {001} terraces in the [$\bar{5}$01] direction. All terraces reconstruct into short dimer rows (though only two dimers long). The zigzag steps are alternately composed of short segments of S_A steps (solid lines) and rebonded S_B steps (dashed lines) in the [010] direction. The (105) unit cell is outlined by a rectangle with dimension of $2a \times \sqrt{6.5}a$ (here a is the lattice constant of Si (5.39 Å)). Because of the large unit cell and large surface undulations in the Ge/Si(105) surface, the PES is rather complex, involving multiple binding sites and diffusion pathways, as evidenced in Fig. 2b.

Several adsorption sites of interest on the Ge/Si(105)-(1×2) surface are indicated in Fig. 2. (Same letters with different subscripts denote equivalent positions due to the symmetry of the surface.) Same as on the flat (001) surfaces [20,21], the most stable binding sites for both Ge and Si adatoms are located at the denoted M-type sites with the adatom saturating one dangling bond each on two adjacent dimers on two terraces. The binding energies of Ge and Si adatom are −4.50 and −5.19 eV, respectively. The relative energies of other important local minimum sites (F, H, P, Q, and C) are presented in Table 2. One notices that, at all the binding sites, the Ge adatom binds less strongly to the Ge/Si(105) surface as compared with the binding of Si adatom on the same surface, which can be understood in terms of the stronger Ge–Si bond than the Ge–Ge bond.

We now present our calculated results about Ge(Si) adatom diffusion on Ge/Si(105) surface. The complex PES (see Fig. 2b) gives a preview of the nature of the diffusion process but do not definitely describe the diffusion rates. To get some quantitative insight into the adatom diffusion, we particularly identify two possible low-barrier pathways for diffusion along the [$\bar{5}$01] and [010] directions (dashed lines in Fig. 2). The potential energies along these two pathways for Ge and Si adatom diffusion on Ge/Si(105) surface are plotted in Figs. 5 and 6, respectively.

Let's first analyze the diffusion barriers along the [$\bar{5}$01] direction (Figs. 5a and 6a), which is physically more relevant direction representing adatoms climbing up and down the hut island. It is interesting to find that the Ge adatom can easily step up and down the S_A steps along the [$\bar{5}$01] direction at typical growth temperatures, following the pathway of $M_1H_1P_1M_2H_2P_2M_1$, with the activation barrier of 0.61 eV, which happens to be very close to the diffusion barrier of 0.617 eV along the dimer rows on the Si(001) surface [21]. This is in sharp contrast with what occurs on (001) surface where the adatoms must overcome a relatively large Schwoebel barrier to across the single
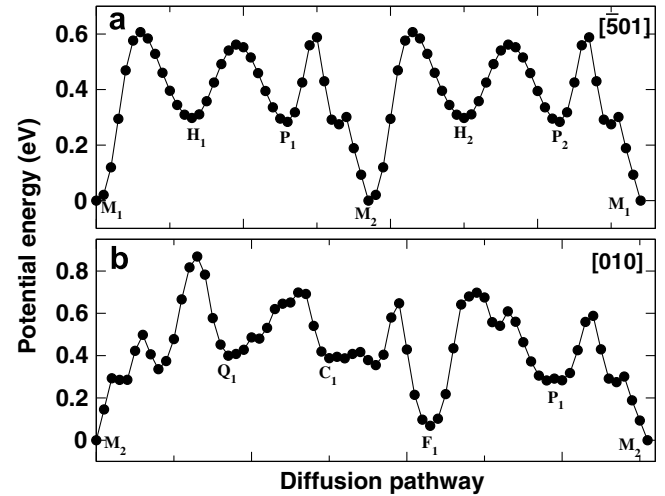
Fig. 5. The potential energies along the diffusion pathways of a Ge adatom on Ge/Si(105)-(1×2) surface: (a) diffusion pathway along the [$\bar{5}$01] direction and (b) diffusion pathway along the [010] direction.
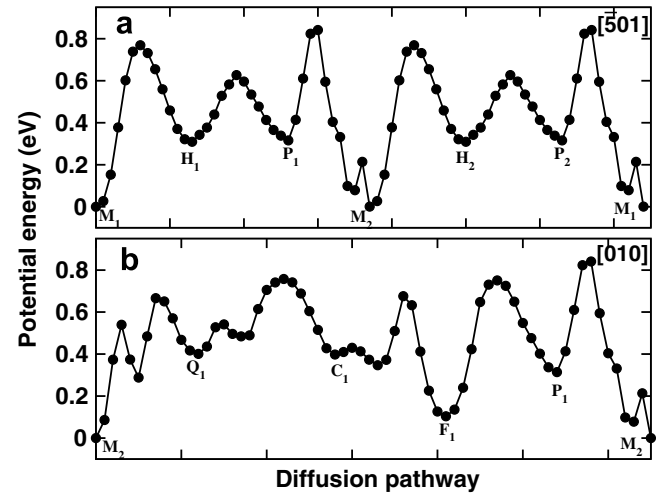
Fig. 6. Same as Fig. 5 for the potential energies along the diffusion pathways for a Si adatom on Ge/Si(105)-(1×2) surface.

height steps [24]. For Si adatom, the activation barrier along this path is relatively higher (0.83 eV). Again, this difference is in accordance with an enhanced bonding between Si and Ge. The fast adatom diffusion along the [$\bar{5}$01] direction on Ge/Si(105) surface is helpful to facilitate the growth of strained Ge and SiGe islands.

The diffusion along the [010] direction, i.e., alongside the zigzag step (S_A and S_B) edges, means adatoms circulating around the hut island following the pathway of $M_2Q_1C_1F_1P_1M_2$ (Figs. 5b and 6b). The activation barriers for Ge and Si adatom are 0.86 and 0.84 eV, respectively, for the rate-limiting step $M_2 \rightarrow Q_1$ and $P_2 \rightarrow M_2$, respectively, which are only slightly larger than that along [$\bar{5}$01] direction. This indicates that for both Ge and Si, the overall adatom diffusion on Ge/Si(105) surface is almost isotropic along both [010] and [$\bar{5}$01] directions, in sharp contrast to that on clean Si(001), where the Si(Ge)

adatom diffusion is highly anisotropic with the preferable diffusion taking place along the dimer rows. This result is in good agreement with another first-principles study of adatom self-diffusion on Ge(105) surface [10], which also showed this isotropic diffusion behavior.

These adatom diffusion processes presented above, on both the wetting layer and the island surfaces, enabled us to give possible kinetic explanations for some experimental observations as discussed before [16], such as the nonuniform alloy concentration due to surface mobility difference between Ge and Si adatoms [27,28].

4. Summary

In summary, we report a comprehensive first-principles total-energy study of Si and Ge adatom binding and diffusion on Ge/Si(001)-(2 × 8) and Ge/Si(105)-(1 × 2) surfaces. We reveal the role played by the rebonded missing dimers on Ge/Si(001)-(2 × 8) surface and the alternate S_A and rebonded S_B steps on Ge/Si(105)-(1 × 2) surface in influencing adatom kinetics by comparison with their dynamic behaviors on flat or stepped Si(001) surface. We discuss some possible implications of our computational results in epitaxial growth of Ge and SiGe films and islands on Si(001) substrates. For example, the enhanced island nucleation rate on Ge-covered Si(001) surface due to repulsive interaction between adatom and dimer vacancy, and the growth of hut island via isotropic fast diffusion on strained Ge(105).

Acknowledgements

References

[1] For review, see e.g., Feng Liu, Fang Wu, M.G. Lagally, Chem. Rev. 97 (1997) 1045.
[2] For review, see e.g. Feng Liu, M.G. Lagally, Surf. Sci. 386 (1997) 169.
[3] X. Chen, F. Wu, Z. Zhang, M.G. Lagally, Phys. Rev. Lett. 73 (1994) 850.
[4] Feng Liu, M.G. Lagally, Phys. Rev. Lett. 76 (1996) 3125.
[5] Y.-W. Mo, D.E. Savage, B.S. Swartzentruber, M.G. Lagally, Phys. Rev. Lett. 65 (1990) 1020.
[6] F. Iwawaki, M. Tomitori, O. Ishikawa, Surf. Sci. Lett. 253 (1991) L411.
[7] J. Tersoff, Appl. Surf. Sci. 188 (2002) 1.
[8] C. Roland, G.H. Gilmer, Phys. Rev. B 47 (1993) 16286.
[9] B.D. Yu, A. Oshiyama, Phys. Rev. B 52 (1995) 8337.
[10] F. Montalenti, D.B. Migas, F. Gamba, Leo Miglio, Phys. Rev. B 70 (2004) 245315.
[11] K. Khor, S. das Sarma, J. Vac. Sci. Technol. A 15 (1995) 1051.
[12] P. Raiteri, D.B. Migas, L. Miglio, A. Rastelli, H. vol Känel, Phys. Rev. Lett. 88 (2002) 256103.
[13] Y. Fujikawa, K. Akiyama, T. Nagao, T. Sakurai, M.G. Lagally, T. Hashimoto, Y. Morikawa, K. Terakura, Phys. Rev. Lett. 88 (2002) 176101.
[14] C.V. Ciobanu, V.B. Shenoy, C.Z. Wang, K.M. Ho, Surf. Sci. 544 (2003) L715.
[15] T. Eguchi et al., Phys. Rev. Lett. 93 (2004) 266102.
[16] Li Huang, Feng Liu, Guang-Hong Lu, X.G. Gong, Phys. Rev. Lett. 96 (2006) 16103.
[17] G. Kresse, J. Hafner, Phys. Rev. B 49 (1994) 14251;
G. Kresse, J. Furthmüller, Comput. Mater. Sci. 6 (1994) 15.
[18] D. Vanderbilt, Phys. Rev. B 41 (1990) 7892;
G. Kresse, J. Hafner, J. Phys. Condens. Matter 6 (1994) 8245.
[19] H.J. Monkhorst, J.D. Pack, Phys. Rev. B 13 (1976) 5188.
[20] D.J. Shu, Feng Liu, X.G. Gong, Phys. Rev. B 64 (2001) 245410.
[21] L. Huang, Feng Liu, X.G. Gong, Phys. Rev. B 70 (2004) 155320.
[22] H. Jonsson, G. Mills, K.W. Hacobsen, in: B.J. Berne, G. Ciccotti, D.F. Coker (Eds.), Classical and Quantum Dynamics in Condensed Phase Simulations, World Scientific, 1998 (Chapter 16).
[23] Guang-Hong Lu, Feng Liu, Phys. Rev. Lett. 94 (2005) 176103.
[24] Q.-M. Zhang, C. Roland, P. Boguslawski, J. Bernhole, Phys. Rev. Lett. 75 (1995) 101.
[25] G.M. Dalpian, A. Fazzio, Antônio J.R. da Silva, Phys. Rev. B 63 (2001) 205303.
[26] A. Vailionis, B. Cho, G. Glass, P. Desjardins, D.G. Cahill, J.E. Greene, Phys. Rev. Lett. 85 (2000) 3672.
[27] J. Stangl et al., Appl. Phys. Lett. 79 (2001) 1474.
[28] Ph. Sonnet, P.C. Kelires, Phys. Rev. B 66 (2002) 205307.